
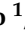

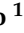



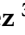



Article

Influences of the Temperature on the Electrical Properties of HfO₂-Based Resistive Switching Devices

Héctor García ^{1,*} , Jonathan Boo ¹ , Guillermo Vinuesa ¹ , Óscar G. Ossorio ¹ , Benjamín Sahelices ² , Salvador Dueñas ¹ , Helena Castán ¹ , Mireia B. González ³  and Francesca Campabadal ³ 

¹ Departamento Electricidad y Electrónica, University of Valladolid, Paseo de Belén 15, 47011 Valladolid, Spain; jonathan.boo@alumnos.uva.es (J.B.); guillermo.vinuesa@alumnos.uva.es (G.V.); ogonoss@ribera.tel.uva.es (Ó.G.O.); sduenas@ele.uva.es (S.D.); helena@ele.uva.es (H.C.)

² Departamento Informática, University of Valladolid, Paseo de Belén 15, 47011 Valladolid, Spain; benja@infor.uva.es

³ Institut de Microelectrònica de Barcelona, IMB-CNM (CSIC), Campus UAB, 08193 Barcelona, Spain; mireia.bargallo.gonzalez@csic.es (M.B.G.); francesca.campabadal@imb-cnm.csic.es (F.C.)

* Correspondence: hecgar@ele.uva.es

Abstract: In the attempt to understand the behavior of HfO₂-based resistive switching devices at low temperatures, TiN/Ti/HfO₂/W metal–insulator–metal devices were fabricated; the atomic layer deposition technique was used to grow the high-k layer. After performing an electroforming process at room temperature, the device was cooled in a cryostat to carry out 100 current–voltage cycles at several temperatures ranging from the “liquid nitrogen temperature” to 350 K. The measurements showed a semiconducting behavior in high and low resistance states. In the low resistance state, a hopping conduction mechanism was obtained. The set and reset voltages increased when temperature decreased because the thermal energies for oxygen vacancies and ions were reduced. However, the temperature did not influence the power absorbed in the reset transition, indicating the local temperature in the filament controls the transition. The set transition turned from gradual to abrupt when decreasing the temperature, due to a positive feedback between the current increase and the Joule heating at low temperatures.

Keywords: resistive switching; ReRAM devices; neuromorphic computing; conduction mechanisms



Citation: García, H.; Boo, J.; Vinuesa, G.; G. Ossorio, Ó.; Sahelices, B.; Dueñas, S.; Castán, H.; González, M.B.; Campabadal, F. Influences of the Temperature on the Electrical Properties of HfO₂-Based Resistive Switching Devices. *Electronics* **2021**, *10*, 2816. <https://doi.org/10.3390/electronics10222816>

Academic Editor: Fabian Khatieb

Received: 27 October 2021

Accepted: 15 November 2021

Published: 17 November 2021

Publisher's Note: MDPI stays neutral with regard to jurisdictional claims in published maps and institutional affiliations.



Copyright: © 2021 by the authors. Licensee MDPI, Basel, Switzerland. This article is an open access article distributed under the terms and conditions of the Creative Commons Attribution (CC BY) license (<https://creativecommons.org/licenses/by/4.0/>).

1. Introduction

The phenomenon of bipolar resistive switching based on the valence change mechanism (VCM) has been attracting great attention in recent years [1,2]. In these devices, a conductive filament (CF) due to oxygen vacancies can be formed and ruptured by applying voltage or current signals. Due to their simple structure, high operation speed, good endurance, and low power consumption, they are currently considered to be one of the next-generation alternatives to traditional non-volatile memories [3,4]. The information in the VCM cells can be encoded in different resistance states, obtaining analog-like multilevel operation. This behavior allows the use of these devices for the implementation of artificial neuronal synapses in neuromorphic systems, since the synaptic weight between two neurons can be electrically adjusted [5]. Various materials have been studied as resistive switching devices, such as perovskites [6], manganites [7], and even organic materials [8]. However, metal oxides are the most widely studied materials [9]. Among them, HfO_x-based devices have been found to be highly scalable, CMOS compatible, and robust; and they are capable of ultrafast and low-energy consumption operation [10,11]. In low-temperature applications, such as aerospace applications, the lack of low-cost, high-density, and durable NVM has been a main limiting factor [12].

The behavior of HfO_x-based resistive switching devices at low temperatures is important, not only to know the switching capability and stability at low temperatures, but also

to study the conduction mechanism in the high-k layer. Previous research often showed temperature measurements in order to address the conduction mechanisms of the samples studied [13,14], establish whether the devices show ohmic or hopping conduction, etc. A study conducted by Kumar Lata et al. showed almost no resistance state temperature dependence at high temperatures (300–450 K) [15]. Another study at high temperatures but in a small temperature range showed no definitive evidence for temperature dependence [13]. A relevant study performed by Walczyk et al. [16] on HfO₂ devices in the 213–413 K range showed that LRS increased with temperature, whereas HRS decreased with rising T, meaning that the resistance ratio greatly reduced as the temperature grew. However, not many studies on the low-temperature characteristics of HfO₂ devices can be found. A study on Ti/Hf/HfO₂/Au in the 100–200 K range showed that the resistance increased as the temperature decreased [17]. A report on Cu-doped HfO₂ films showed that the LRS increased with temperature, whereas the HRS decreased as the temperature rose [18]. Finally, a study on HfO₂ and HfO_x devices conducted by Molina et al. showed that the HRS increased as the temperature dropped [19].

In this work, our objective was studying the electrical properties of HfO₂-based metal–insulator–metal structures by measuring current–voltage resistive switching cycles at several temperatures ranging from “liquid nitrogen temperature” to 350 K. We focused our attention on the conduction mechanisms and the influences of the temperature on set and reset transitions.

2. Experimental

In order to carry out our study, TiN/Ti/HfO₂/W metal–insulator–metal devices were used as resistive switching devices. The fabrication process started with the deposition of a 20 nm-thick Ti adherence layer on a 100 mm-diameter Si-n⁺⁺ wafer, followed by the deposition of a 50 nm-thick W layer. Both layers were grown by magnetron sputtering. Next, a 100 nm SiO₂ isolation oxide was grown by plasma-enhanced chemical vapor deposition (PECVD) using SiH₄ as the precursor, and then patterned by photolithography and dry etching. The apertures in the SiO₂ layer define the active area of the MIM devices. After the active area definition, the 10 nm HfO₂ film was deposited by atomic layer deposition (ALD) at 225 °C using TDMAH and H₂O as precursors and N₂ as the carrier and purge gas. The top electrode, consisting of a metal layer of 10 nm-thick Ti and 200 nm-thick TiN, was then grown by magnetron sputtering and patterned by a lift-off process. Finally, a 500 nm Al layer was deposited on the back of the wafer by magnetron sputtering for electrically contacting the W bottom electrode through the Si-n⁺⁺ substrate. Devices with an area of $1.44 \times 10^4 \mu\text{m}^2$ were used to perform the electrical measurements. Figure 1 shows a cross-section picture of our devices.

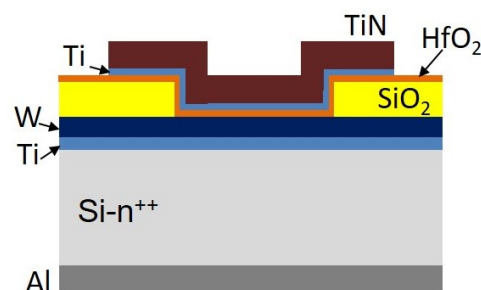


Figure 1. Cross-section picture of our resistive switching devices.

The current–voltage (I–V) measurements were carried out using a Hewlett-Packard Semiconductor Parameter Analyzer (model 4155B). The measurements were performed at several temperatures ranging from liquid nitrogen temperature (≈ 78 K) to 350 K. Devices were first cooled in darkness using an Oxford Instruments cryostat (model DM1710), and an Oxford Instruments temperature controller (model ITC 503) was used to monitor and to

control the temperature during the measurements. One hundred current–voltage cycles were measured at each temperature (78, 100, 125, 150, 200, 225, 250, 275, 300, 325, and 350 K); we started the measurements at the lowest temperature. The equipment was connected to a computer using a GPIB interface and was controlled using Agilent VEE software.

3. Results and Discussion

The fabricated devices showed bipolar resistive switching behavior, as shown in Figure 2 for the 300 K measurements, with set and reset transitions at positive and negative voltages, respectively. Together with the 100 cycles measurements, we have represented the average in red. These devices were previously studied, and filamentary conduction was observed. The resistive switching mechanism was found to be valence change memory effect (VCM) [20]. In this mechanism, the conductive filaments are due to oxygen vacancies [21]. The oxygen reservoir capability of Ti is well known. It is able to attract/release oxygen from/to the HfO₂ layer during the reversible I–V cycles [22]. This oxygen ion migration was responsible for the formation of percolation paths made of oxygen vacancies. An initial electroforming process was necessary to form the conductive filaments in our devices. We performed the electroforming at room temperature before cooling the device, and a current compliance of 200 μ A was used during the forming process to prevent irreversible oxide breakdown.

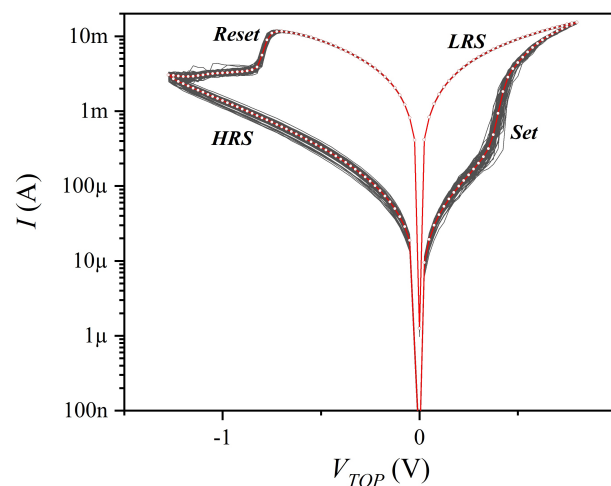


Figure 2. Current–voltage cycles measured at 300 K (black lines) and the 100-cycle average (red line).

Figure 3 shows the resistance value's cumulative probability in the low resistance state (R_{on}) at the temperatures used in this work. The cycle-to-cycle variability was not significant: it is known the low resistance state (LRS) variability worsens when a compliance current is used in the set transition [3], but we did not use any compliance in our I–V measurements. We observed a semiconducting (or non-metallic) behavior in the LRS because the resistance value decreased when temperature increased. Usually, resistive switching devices at LRS show metallic behavior or hopping conduction. For conductive bridge devices (CBRAMs), metallic behavior is obtained because the conductive filament is caused by metal ions, as has been observed by microscopy several years ago [23]. However, VCM devices can show either metallic or hopping conduction, depending on the concentration of oxygen vacancies [24]. For instance, metallic behavior was observed in TiN/HfO₂/Ti/TiN capacitors [16], and non-metallic was observed in TiN/HfAlO_x/Pt structures [12], although metallic behavior was observed in the latter case for breakdown devices, where very high concentrations of oxygen vacancies were present. We can observe the current in the LRS was thermally activated. These processes usually follow an Arrhenius law, indicating the existence of an activation energy (E_a). The use of $\ln(I_{on})$ vs. $1/kT$ relationship allowed us to obtain an activation energy value, as we have represented in Figure 4a for $V_{TOP} = +0.1$ V. We can observe the current reached a saturation value at low

temperatures. As the current was due to hopping via traps created by oxygen vacancies, electron thermal energy was not high enough at low temperatures to hop between nearest neighbor traps.

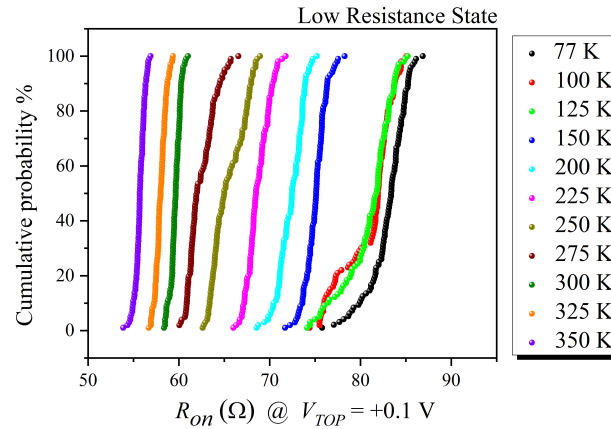


Figure 3. R_{on} @ $V_{TOP} = +0.1$ V cumulative probability measured at different temperatures ranging from 78 K to 350 K.

On the other hand, the equation of hopping conduction is [25]:

$$I = qANav_0 \exp\left(\frac{-E_T}{kT}\right) \exp\left(\frac{qaV}{2dkT}\right), \tag{1}$$

where q is the electron charge, A is the area, N is the density of space charge, a is the average of hopping distance, v_0 is the intrinsic vibration frequency, E_T is the barrier height of hopping, k is the Boltzmann constant, T is the temperature, d is the oxide film thickness, and V is the voltage applied to the top electrode. The activation energy E_a can be expressed as $E_T - qaV/2d$, so if we represent the activation energy for different applied voltages, we can obtain the barrier height of hopping as the intercept of vertical axes. We have represented the E_a vs. V_{TOP} plot in Figure 4b, and we obtained a barrier height of 11.9 meV. R. Fang et al. found E_T values ranging from 6 to 54 meV depending on the resistance state in TiN/HfAlO_x/Pt capacitors [12], a value with the same order of magnitude as our result. Moreover, the slope of the fitting line shown in Figure 4b allowed us to obtain the average of hopping distance in the LRS. The value obtained is 0.3 nm, a similar value than the one obtained by K-H. Chen et al., who obtained a value of 1.44 nm when using a 10 μA compliance current and a value of 0.3 nm when using a 100 μA compliance current, in zinc-doped SiO₂-based resistive switching devices [25].

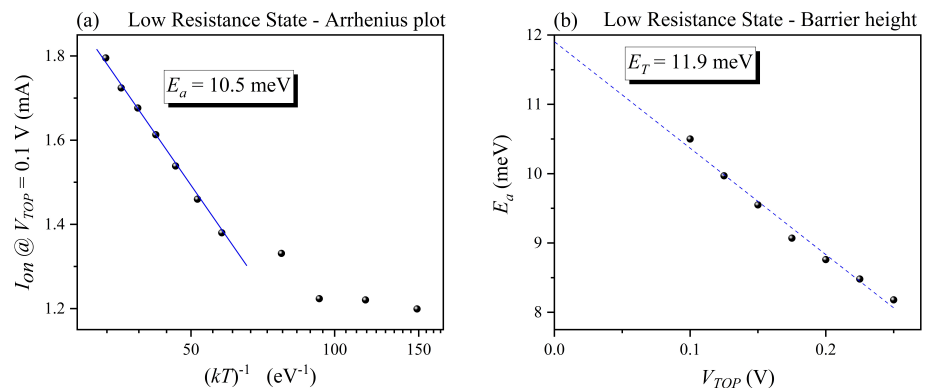


Figure 4. Arrhenius plot (a), and barrier height of hopping and average hopping distance (b).

Figure 5 shows the resistance value's (R_{off}) cumulative probability in the high resistance state (HRS). Cycle-to-cycle variability was larger than in the LRS case. The variability is attributed to a change in the number of oxygen vacancies in the CF due to the stochastic nature of formation and rupturing during the set and reset transitions. The indeterminate tunneling gap formed in the reset process is responsible for the variability of R_{off} [26]. Although temperature dependence can be observed in HRS, the cycle-to-cycle variability makes it difficult to study this dependence. Different mechanisms have been proposed for the conduction in HRS, such as Poole–Frenkel emission [27], tunneling [28], and Schottky emission [29].

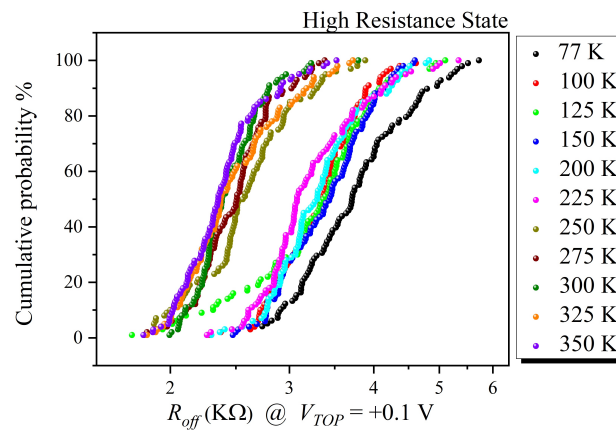


Figure 5. R_{off} @ $V_{TOP} = +0.1$ V cumulative probability measured at different temperatures ranging from 78 K to 350 K.

Figure 6a shows the reset voltage (V_{res}) as a function of the temperature. The reset voltage has been obtained as the point having the maximum current in the reset process. Each point in the graph corresponds to the mean value of 100 I–V cycles and is plotted together with standard error bars. The reset voltage's cycle-to-cycle variability was almost negligible, mainly, at room and higher temperatures. However, there is a clear temperature dependence: V_{res} increases as temperature decreases. This trend is usually related to the thermal energies of oxygen vacancies: as the temperature cools down, a stronger electric field is needed to form or to rupture the conductive filaments because the thermal energies for oxygen vacancies and ions are reduced [12]. In a recent work, we observed, in measurements performed at room temperature, that set and reset transitions, and even intermediate resistance states, could be controlled by the power absorbed by the devices [30]. Figure 6b shows the power absorbed by the devices in the reset transition as a function of the temperature. We have also added standard error bars. The error increased for low temperatures due to a greater dispersion in the resistance values (see Figure 3). The power was always about 8 mW regardless of the temperature value. This result implies the reset is a Joule process: the conductive filament rupture is controlled by its local temperature. The temperature influences the resistance value in LRS (R_{on}) because, as explained, hopping conduction is a thermally activated process. Higher temperatures imply lower R_{on} values, and as $V_{res} = \sqrt{P/R_{on}}$, lower voltage values are necessary to obtain the power necessary to attract oxygen ions from the Ti layer. We saw in Figure 4a that the current in LRS (I_{on}) saturates at low temperatures. However, the reset power value (P_{reset}) remains constant despite the saturation I_{on} value at low temperatures, because V_{reset} becomes constant at temperatures near the liquid nitrogen one (see Figure 4a).

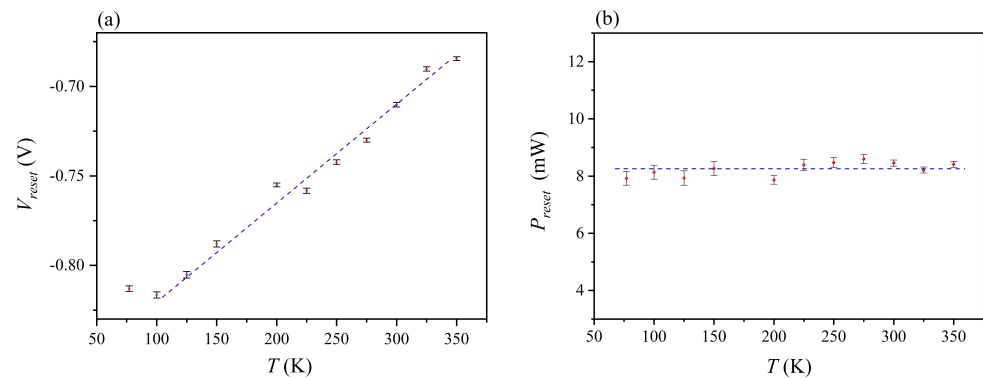


Figure 6. Reset voltage, V_{res} , (a) and reset power, P_{res} , (b) measured for the different temperatures. Each point corresponds to the mean value of 100 I–V cycles.

Regarding the set voltage, Figure 7 shows V_{set} for the different temperatures. The set voltage has been defined as the applied voltage whose derivative value reaches a fixed value. As for the reset voltage, each point in the graph corresponds to the mean value of 100 I–V cycles and is plotted together with standard error bars. The temperature dependence was similar that the one observed in the reset case: V_{set} increased as temperature decreased, because, as stated before, the thermal energies for oxygen vacancies and ions were reduced. However, although the cycle-to-cycle variability was small at high temperatures, in this case it increased when temperature decreased, as standard error bars indicate in Figure 7. The stochastic formation of the CF was clearly enhanced at low temperatures. In the reset case, we did not see such high cycle-to-cycle variability at low temperatures, perhaps because the high current flowing through the filaments just before the reset increased the local temperature.

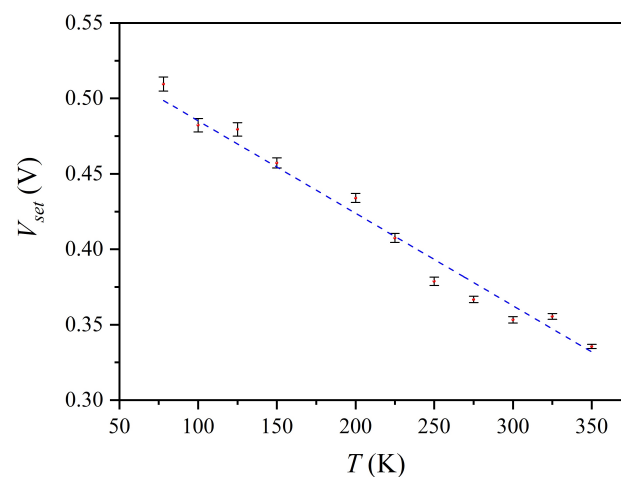


Figure 7. Set voltage, V_{set} , mean value of 100 I–V cycles.

In order to show the differences in the set transition at low and high temperatures, 100 I–V cycles at positive V_{TOP} voltages are represented in Figure 8 for 100 K (as an example of low temperature) and 350 K (as an example of high temperature). In the case of $T = 100$ K, we can observe different bands which have been plotted using red and black for a clear visualization. These bands are only a measurement artifact due to the voltage step used in the I–V measurements (25 mV). This voltage is the minimum interval between two consecutive bands. If a lower voltage step had been used, a greater number of bands would have been obtained and the bands would have been closer. There is another issue regarding the set transition. It is an abrupt transition for low temperatures, but it turns into a gradual transition for temperatures higher than about 200 K, as represented in Figure 8

in blue for the 350 K measurements. The abrupt switching events are related to a positive feedback between the current increase and the Joule heating [31,32]. The current increment was able to increase the local temperature, which caused a faster change in the oxygen vacancies concentration, and thereby increased the current again. At temperatures higher than about 200 K, the abrupt transitions disappeared. At these temperatures, the thermal energy for oxygen vacancies was high enough so they could move from or to the Ti layer at enough low voltages to obtain gradual set transitions. However, at lower temperatures, stronger electric fields were required to form the filament, suddenly increasing the power dissipated and the Joule heating. The mean values of the different bands shown in black and red in Figure 8 for the 100 K measurement are represented in Figure 9a. Once the device was in the LRS after performing the set transition, the resistance state was independent of the V_{set} value, as we have represented in Figure 9b. The set transition has been represented as a blue to red color change in Figure 9. After performing the set transition, the red lines overlap regardless the V_{set} value. Hence, the cycle-to-cycle variation was not due to the existence of different conductive filaments, as their shape would probably be different and we would obtain different resistance states depending on which filament is fully formed. The variation seems to be due to the stochastic nature of the switching mechanism.

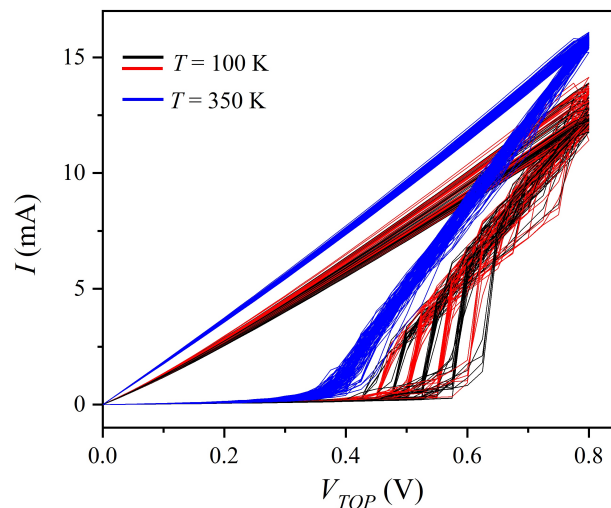


Figure 8. I–V curves at positive voltages for $T = 100$ K (red and black lines) and $T = 350$ K (blue lines).

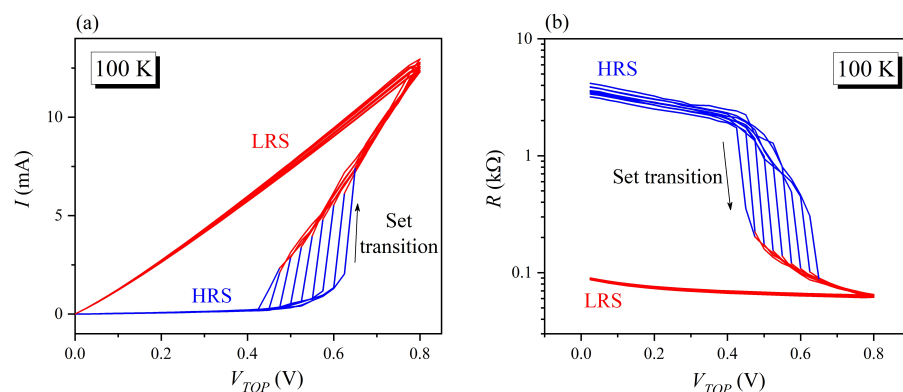


Figure 9. Mean values of the different bands for the I–V characteristic measured at 100 K (a) and the R–V characteristic at 100 K obtained from the mean values of the bands (b).

4. Conclusions

In summary, our study of the electrical properties of TiN/Ti/HfO₂/W resistive switching devices revealed a non-metallic behavior and a hopping conduction mechanism in the

low resistance state. A barrier height value of 11.9 eV and a hopping distance value of 0.3 nm were obtained, values with the same order of magnitude as the ones found in other works. The reset voltage increases at low temperatures; however, the reset transition is a Joule process, as no temperature dependence was found in the power absorbed in this transition. The decrease in the hopping current at low temperatures implies higher V_{res} to keep the power constant. In the case of the set transition, low temperatures increase the set voltage, and also enhance the cycle-to-cycle variability. The set transition changed from a gradual transition at room temperatures to an abrupt transition when devices were cooled to 200 K or lower temperatures. Positive feedback between the current increase and the Joule heating can explain this trend.

Author Contributions: Conceptualization, H.G., S.D., and J.B.; formal analysis, H.G. and J.B.; resources, M.B.G. and F.C.; writing—original draft, H.G.; writing—review and editing, J.B., G.V., Ó.G.O., B.S., S.D., H.C., M.B.G. and F.C. All authors have read and agreed to the published version of the manuscript.

Funding: This research was funded by the Spanish Ministry of Economy and Competitiveness and the FEDER program through projects TEC2017-84321-C4-2-R and TEC2017-84321-C4-1-R.

Conflicts of Interest: The authors declare no conflict of interest.

References

1. Slesazeck, S.; Mikolajick, T. Nanoscale resistive switching memory devices: A review. *Nanotechnology* **2019**, *30*, 352003. [\[CrossRef\]](#)
2. Wang, Z.; Wu, H.; Burr, G.W.; Hwang, C.S.; Wang, K.L.; Xia, Q.; Yang, J.J. Resistive switching materials for information processing. *Nat. Rev. Mater.* **2020**, *5*, 173–195. [\[CrossRef\]](#)
3. Zahoor, F.; Zulkifli, T.Z.A.; Khanday, F.A. Resistive Random Access Memory (RRAM): An Overview of Materials, Switching Mechanism, Performance, Multilevel Cell (mlc) Storage, Modeling, and Applications. *Nanoscale Res. Lett.* **2020**, *15*, 90. [\[CrossRef\]](#) [\[PubMed\]](#)
4. Banerjee, W. Challenges and Applications of Emerging Nonvolatile Memory Devices. *Electronics* **2020**, *9*, 1029. [\[CrossRef\]](#)
5. Chakraborty, I.; Jaiswal, A.; Saha, A.K.; Gupta, S.K.; Roy, K. Pathways to efficient neuromorphic computing with non-volatile memory technologies. *Appl. Phys. Rev.* **2020**, *7*, 021308. [\[CrossRef\]](#)
6. Wu, X.; Yu, H.; Cao, J. Unraveling the origin of resistive switching behavior in organolead halide perovskite based memory devices. *AIP Adv.* **2020**, *10*, 085202. [\[CrossRef\]](#)
7. Román Acevedo, W.; Rubi, D.; Lecourt, J.; Lüders, U.; Gomez-Marlasca, F.; Granel, P.; Golmar, F.; Levy, P. Manganite-based three level memristive devices with self-healing capability. *Phys. Lett. A* **2016**, *380*, 2870–2875. [\[CrossRef\]](#)
8. Cheong, K.Y.; Tayeb, I.A.; Zhao, F.; Abdullah, J.M. Review on resistive switching mechanisms of bio-organic thin film for non-volatile memory application. *Nanotechnol. Rev.* **2021**, *10*, 680–709. [\[CrossRef\]](#)
9. Carlos, E.; Branquinho, R.; Martins, R.; Kiazadeh, A.; Fortunato, E. Recent Progress in Solution-Based Metal Oxide Resistive Switching Devices. *Adv. Mater.* **2020**, *33*, 2004328. [\[CrossRef\]](#) [\[PubMed\]](#)
10. Bersuker, G.; Gilmer, D.C.; Veksler, D. Metal-oxide resistive random access memory (RRAM) technology: Material and operation details and ramifications. In *Advances in NON-Volatile Memory and Storage Technology*; Magyari-Köpe, B., Nishi, Y., Eds.; Elsevier: Amsterdam, The Netherlands, 2019; pp. 35–102. [\[CrossRef\]](#)
11. Giovinazzo, C.; Sandrini, J.; Shahrabi, E.; Celik, O.T.; Lelebizi, Y.; Ricciardi, C. Analog Control of Retainable Resistance Multistates in HfO₂ Resistive-Switching Random Access Memories (ReRAMs). *ACS Appl. Electron. Mater.* **2019**, *1*, 900–909. [\[CrossRef\]](#)
12. Fang, R.; Chen, W.; Gao, L.; Yu, W.; Yu, S. Low-Temperature Characteristics of HfO_x-Based Resistive Random Access Memory. *IEEE Electron. Device Lett.* **2015**, *36*, 567–569. [\[CrossRef\]](#)
13. Liu, Y.; Ouyang, S.; Yang, J.; Tang, M.; Wang, W.; Li, G.; Zou, Z.; Liang, Y.; Li, Y.; Xiao, Y.; et al. Effect of film thickness and temperature on the resistive switching characteristics of the Pt/HfO₂/Al₂O₃/TiN structure. *Solid-State Electron.* **2020**, *173*, 107880. [\[CrossRef\]](#)
14. Rodríguez-Fernández, A.; Aldana, S.; Campabadal, F.; Suñé, J.; Miranda, E.; Jiménez-Molinos, F.; Roldán, J.B.; González, M.B. Resistive Switching with Self-Rectifying Tunability and Influence of the Oxide Layer Thickness in Ni/HfO₂/n⁺-Si. *IEEE Trans. Electron. Devices* **2017**, *64*, 3159–3166. [\[CrossRef\]](#)
15. Kumar Lata, L.; Jain, P.K.; Chand, U.; Bhatia, D.; Shariq, M. Resistive switching characteristics of HfO₂ based bipolar non-volatile RRAM cell. In *Materials Today: Proceedings*; Arora, M., Kumar Jain, P., Zafar, R., Vyas, R., Eds.; Elsevier: Amsterdam, The Netherlands, 2020; Volume 30, pp. 217–220. [\[CrossRef\]](#)
16. Walczyk, C.; Walczyk, D.; Schroeder, T.; Bertaud, T.; Sowinska, M.; Lukosius, M.; Fraschke, M.; Wolansky, D.; Tillack, B.; Miranda, E.; et al. Impact of Temperature on the Resistive Switching Behavior of Embedded HfO₂-Based RRAM Devices. *IEEE Trans. Electron. Devices* **2011**, *58*, 3124–3131. [\[CrossRef\]](#)

17. Nakajima, R.; Azuma, A.; Yoshida, Y.; Shimizu, T.; Ito, T.; Shingubara, S. Hf layer thickness dependence of resistive switching characteristics of Ti/Hf/HfO₂/Au resistive random access memory device. *Jpn. J. Appl. Phys.* **2018**, *57*, 06HD06. [[CrossRef](#)]
18. Wang, Y.; Liu, Q.; Long, S.; Wang, W.; Zhang, M.; Zhang, S.; Li, Y.; Zuo, Q.; Yang, J. Investigation of resistive switching in Cu-doped HfO₂ thin film for multilevel non-volatile memory applications. *Nanotechnology* **2009**, *21*, 045202. [[PubMed](#)]
19. Molina, J.; Torres, R.; Ranjan, A.; Pey, K.-L. Resistive switching characteristics of MIM structures based on oxygen-variable ultra-thin HfO₂ and fabricated at low temperature. *Mater. Sci. Semicond. Process.* **2017**, *66*, 191–199. [[CrossRef](#)]
20. González-Cordero, G.; González, M.B.; García, H.; Campabadal, F.; Dueñas, S.; Castán, H.; Jiménez-Molinos, F.; Roldán, J.B. A physically based model for resistive memories including a detailed temperature and variability description. *Microelectron. Eng.* **2017**, *178*, 26–29. [[CrossRef](#)]
21. Waser, R.; Dittmann, R.; Staikov, G.; Szot, K. Redox-Based Resistive Switching Memories—Nanoionic Mechanisms, Prospects, and Challenges. *Adv. Mater.* **2009**, *21*, 2632–2663. [[CrossRef](#)]
22. Fang, Z.; Wang, X.P.; Sohn, J.; Weng, B.B.; Zhang, Z.P.; Chen, Z.X.; Tang, Y.Z.; Lo, G.-Q.; Provine, J.; Wong, S.S.; et al. The Role of Ti Capping Layer in HfO_x-Based RRAM Devices. *IEEE Electron. Device Lett.* **2014**, *35*, 912–914. [[CrossRef](#)]
23. Guo, X.; Schindler, C.; Menzel, S.; Waser, R. Understanding the switching-off mechanism in Ag⁺ migration based resistively switching model systems. *Appl. Phys. Lett.* **2007**, *91*, 133513. [[CrossRef](#)]
24. Wang, C.; Wu, H.; Gao, B.; Zhang, T.; Yang, Y.; Qian, H. Conduction mechanisms, dynamics and stability in ReRAMs. *Microelectron. Eng.* **2018**, *187*, 121–133. [[CrossRef](#)]
25. Chen, K.-H.; Zhang, R.; Chang, T.-C.; Tsai, T.-M.; Chang, K.-C.; Lou, J.C.; Young, T.-F.; Chen, J.-H.; Shih, C.-C.; Tung, C.-W.; et al. Hopping conduction distance dependent activation energy characteristics of Zn:SiO₂ resistance random access memory devices. *Appl. Phys. Lett.* **2013**, *102*, 133503. [[CrossRef](#)]
26. Xu, X.-X.; Luo, Q.; Gong, T.-C.; Lv, H.-B.; Liu, Q.; Liu, M. Resistive switching memory for high density storage and computing. *Chin. Phys. B* **2021**, *30*, 058702. [[CrossRef](#)]
27. Kim, Y.-M.; Lee, J.-S. Reproducible resistance switching characteristics of hafnium oxide-based nonvolatile memory devices. *J. Appl. Phys.* **2008**, *104*, 114115. [[CrossRef](#)]
28. Yu, S.; Guan, X.; Wong, H.-S.P. Conduction mechanism of TiN/HfO_x/Pt resistive switching memory: A trap-assisted-tunneling model. *Appl. Phys. Lett.* **2011**, *99*, 0635507. [[CrossRef](#)]
29. Lin, C.-Y.; Wang, S.-Y.; Lee, D.-Y.; Tseng, T.-Y. Electrical Properties and Fatigue Behaviors of ZrO₂ Resistive Switching Thin Films. *J. Electrochem. Soc.* **2008**, *155*, H615–H619. [[CrossRef](#)]
30. García, H.; Vinuesa, G.; Ossorio, O.G.; Sahelices, B.; Castán, H.; Dueñas, S.; González, M.B.; Campabadal, F. Study of the set and reset transitions in HfO₂-based ReRAM devices using a capacitor discharge. *Solid-State Electron.* **2021**, *183*, 108113. [[CrossRef](#)]
31. Fleck, K.; La Torre, C.; Aslam, N.; Hoffmann-Eifert, S.; Böttger, U.; Menzel, S. Uniting Gradual and Abrupt SET Processes in Resistive Switching Oxides. *Phys. Rev. Appl.* **2016**, *6*, 064015. [[CrossRef](#)]
32. Cüppers, F.; Menzel, S.; Bengel, C.; Hardtdegen, A.; von Witzleben, M.; Böttger, U.; Waser, R.; Hoffmann-Eifert, S. Exploiting the switching dynamics of HfO₂-based ReRAM devices for reliable analog memristive behavior. *APL Mater.* **2019**, *7*, 091105. [[CrossRef](#)]